Research Square

Preprints are preliminary reports that have not undergone peer review. They should not be considered conclusive, used to inform clinical practice, or referenced by the media as validated information.

Origin of the p-type characteristics of organic semiconductors

Wenping Hu (huwp@tju.edu.cn)
Tianjin University https://orcid.org/0000-0001-5686-2740
Liqiang Li
Tianjin University https://orcid.org/0000-0001-8399-3957
Yinan Huang
Tianjin University
Xiaosong Chen
Tianjin University
Kunjie Wu
Chinese Academy of Sciences
Yajing Sun
Tianjin University
Zhongwu Wang
Tianjin University
Yongxu Hu
Tianjin University
Liqian Yuan
Tianjin University
Shuguang Wang
Tianjin University
Jie Li
Tianjin University
Deyang Ji
Tianjin University https://orcid.org/0000-0002-8206-3130
Xiaotao Zhang
Tianjin University

Physical Sciences - Article

Keywords: Organic semiconductors, oxygen-induced organic radical cations, plasma de-doping

Posted Date: November 23rd, 2021

DOI: https://doi.org/10.21203/rs.3.rs-1029314/v1

License: This work is licensed under a Creative Commons Attribution 4.0 International License.
Read Full License

Origin of the p-type characteristics of organic semiconductors

Liqiang Li[1,2#], Yinan Huang[1#], Xiaosong Chen[1], Kunjie Wu[2], Yajing, Sun[1], Zhongwu Wang[1], Yongxu Hu[1], Liqian Yuan[1], Shuguang Wang[1], Jie Li[1], Deyang Ji[1], Xiaotao Zhang[1], and Wenping Hu[1,2*]

[1]Tianjin Key Laboratory of Molecular Optoelectronic Sciences, Department of Chemistry, Institute of Molecular Aggregation Science, Tianjin University, Tianjin 300072, China

[2]Joint School of National University of Singapore and Tianjin University, International Campus of Tianjin University, Binhai New City, Fuzhou 350207, China

[3]Suzhou Institute of Nano-Tech and Nano-Bionics (SINANO), Chinese Academy of Sciences, Suzhou, Jiangsu 215123, China

[#]These authors contributed equally to this work

Correspondence and requests for materials should be addressed to W.H.

(Email: huwp@tju.edu.cn)

Organic semiconductors (OSC) are generally considered intrinsic (undoped)[1-3], an assumption which underpins our understanding of the charge transport in this promising class of materials. However, this premise conflicts with a variety of experimental observations, that suggest the presence of excess holes carriers in OSCs at room temperature[2,4-10]. Here, using a low-power plasma de-doping method, we report that trace amounts (~10^{15} cm^{-3}) of oxygen-induced organic radical cations (OIORCs) are inherent in the lattice of OSCs as innate hole carriers, and that this is the origin of the p-type characteristics exhibited by the majority of these materials. This finding clarifies previously unexplained organic electronics phenomena[4,5,7,8,11,12] and provides a foundation upon which to re-understand charge transport in OSCs. Furthermore, the de-doping method can eliminate the trace OIORCs, resulting in the complete disappearance of p-type behavior, while re-doping (under light irradiation in O_2), reverses the process. These methods can precisely modulate key electronic characteristics (e.g., conductivity, polarity, and threshold voltage) in a nondestructive way, expanding the explorable charge transport property space for all known OSC materials. Accordingly, we conclude that our tailorable OIORC doping strategy, requiring only off-the-shelf equipment and a glovebox, will become a core technology in the burgeoning organic electronics industry.

With the potential for functional advantages over their inorganic counterparts, OSCs are promising candidates for use in the next generation of electronic devices. Much progress has been made on material design and fabrication[13-19]; however, the origin of the charge transport characteristics is still perplexing. In most inorganic semiconductors, charge transport is governed by the incorporation of extrinsic dopants that are capable of inducing either holes in the valence band or electrons in the conduction band. In contrast, although OSCs are intrinsically ambipolar because of the similar electronic structure of the lowest unoccupied molecular orbital (LUMO) and the highest occupied molecular orbital (HOMO) states[1], the majority of them exhibit unipolar p-type characteristics. This is traditionally attributed to the inhibition of n-type transport by the inefficient injection of electrons by the

mismatched energy levels at the metal-semiconductor junctions[20,21], and the strong electron trapping ability of the acceptor-like localized states of insulator interfaces[22] and oxygen/water[23].

These interpretations are based on the unconfirmed premise that OSCs are intrinsic (undoped). However, despite great experimental efforts, very few OSCs have achieved a balanced ambipolarity[1,24]. Another perplexing fact is that OSCs generally exhibit hole carrier densities in the region of 10^{12}-10^{16} cm^{-3} [6,10] and conductivities of 10^{-8} ~10^{-4} $S{\cdot}cm^{-1}$ [2,9], much higher than what is expected from thermally-activated forbidden transitions at room temperature (the typical bandgap of OSCs of 2-3 eV should yield negligible intrinsic carrier concentrations considering $n_i = \sqrt{N_C N_v} exp\,(-\frac{E_g}{2kT})$)[25]. Furthermore, depletion mode transistors are frequently observed[4,5]. Some spectral investigations suggested that the Fermi level is close to the HOMO in OSCs[7,8], which is similar to the observation of inorganic semiconductors doped by some acceptor impurities. These striking discrepancies suggests the presence of excess hole carriers and imply that previous studies have not revealed the true origin of OSC p-type characteristics, which must originate from acceptor impurities that cause these dominant hole carriers.

Here, we demonstrate that trace oxygen, innately incorporated in the OSC lattice as an acceptor, induces the geminate superoxide anion (SA) and organic radical cation (ORC), and fundamentally endows OSCs with p-type characteristics. This has not been revealed until now due to the lack of a de-doping method to remove the lattice-incorporated trace oxygen (for details, see Supplementary Section 1). Moreover, because, in previous reports, OSCs still showed p-type transporting behavior after the removal of the adsorbed oxygen by vacuum annealing or sublimation[26,27], these characteristics were considered to be inherent, with oxygen doping merely modulating the p-type transport[26-30]. This is the cause of some perplexing observations and the fundamental reason why some classical physical models used in the field are invalid for organic devices. We developed a de-doping method (using a low-power plasma) to eliminate ORC and SA induced by the innate trace oxygen, and a re-doping method (light irradiation in oxygen) to re-generate them, by which OSCs can

be switched between innately doped (p-type) and intrinsic (non-conductive) states reversibly (**Fig. 1a**), revealing the decisive role of the innate trace oxygen in charge transport.

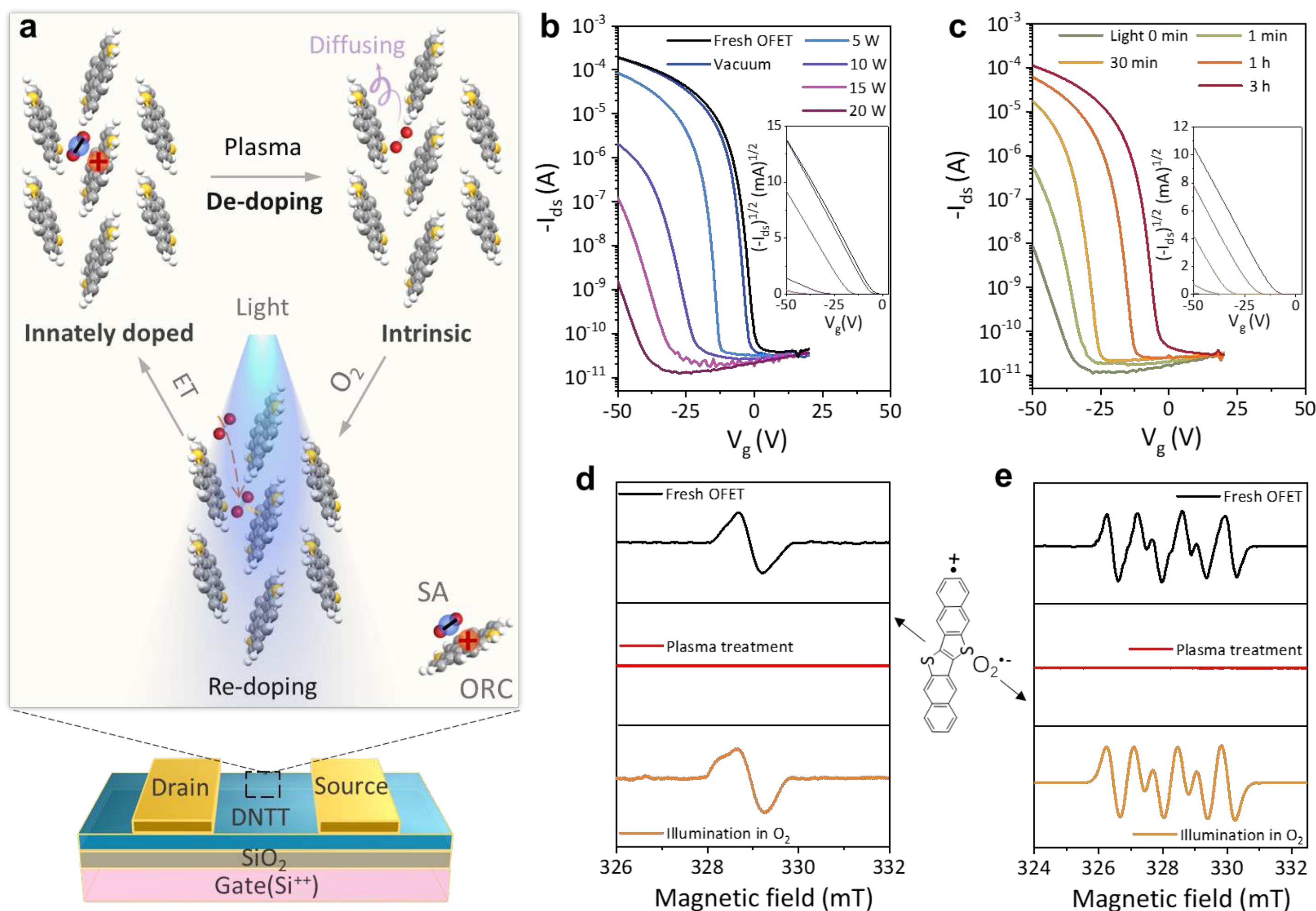

Fig. 1 | Illustration and characteristics of the de-doping and re-doping processes. a, Schematic of the elimination and regeneration of ORC and SA in OSCs incorporated into an OFET structure. When illuminated in O_2, a neutral molecule will be excited and transfer an electron to oxygen, regenerating the geminate ORC and SA. ET denotes electron transfer. **b,** Gradual disappearance of p-type transfer characteristics of the DNTT OFET after plasma treatment. **c**, Gradual recovery of p-type transfer characteristics of the DNTT OFET when illuminated in oxygen. V_{ds} = −50 V in **b and c**. The measurements were performed in the dark. **d, e,** The evolution of the EPR signal of ORC and SA in the process of plasma treatment and illumination in oxygen, showing the reversible disappearance and recovery processes. The detected EPR signal should be ascribed to DMPO-OOH but is described as SA in this work for convenience.

An organic field-effect transistor (OFET, **Fig. 1a**), as a model device sensitive to charge transport, was used to investigate this surprising and unprecedented phenomenon. We firstly selected a classic OSC molecule, dinaphtho[2,3-b:2′,3′-f]thieno[3,2-b]thiophene (DNTT)[31], as the active layer in the fabricated device (for details, see Methods). The fresh OFET was investigated in a home-made

system containing an integrated plasma source, optical window, and environmental control system (*i.e.*, off-the-shelf components) that enabled in-situ measurements (see Supplementary Section 2 and Methods). As shown in **Fig. 1b**, the fresh OFET showed typical p-type transfer characteristics with a saturated mobility of 2 $cm^2 \cdot V^{-1} \cdot s^{-1}$ and a threshold voltage of -5 V in air, and negligible changes in these properties after 6 h in a high vacuum (10^{-4} Pa), indicating that the electrical property of the DNTT OFET was not modified by decreased pressure. Surprisingly, after the short period low-power plasma treatment (see Methods), the transfer curve immediately shifted negatively with a slight decrease in mobility and off-state current. The threshold voltage continued to shift negatively with increasing plasma power, suggesting a reduced carrier density in the channel area induced by the same gate voltage. This change could be explained by the increased energy gap between the Fermi level (E_F) and the HOMO, and E_F pinning (discussed in detail later). Meanwhile, the subthreshold swing and mobility significantly deteriorated, implying the increase of the density of donor-like traps (Supplementary Section 3). When p-type characteristics almost completely disappeared, the conductivity (by two-terminal measurement) was too small to be measurable (Supplementary Section 4).

Despite the drastic change in electrical characteristics, the OFET was not damaged by the low-power plasma. When 1 atm of oxygen was filled in the system for 5 min, p-type characteristics of the OFET recovered slightly (**Fig. 1c**). Upon further extending the time of exposure to oxygen, the rate of recovery remained quite slow. However, when the OFET was illuminated by a full-spectrum Xe lamp in an oxygen atmosphere, its p-type characteristics rapidly recovered, almost to the original level after 3 h (output characteristics of this process are shown in Supplementary Section 5). The process is reversible, suggesting a negligible impact of oxygen (de)intercalation on the ordered lattice; a remarkable result given the general difficulty in doping both inorganic and organic semiconductors without affecting their structure. These results also suggest that the plasma treatment is nondestructive for OSCs at the molecular and aggregate levels, and this was verified by X-ray

diffraction, atomic force microscopy, Raman, infrared, and UV-Vis absorption measurements (Supplementary Section 6). In addition, p-type characteristics are only recoverable in the presence of oxygen (Supplementary Section 7), indicating that it plays a key role in the disappearance and recovery of the p-type characteristics in the above process.

Oxygen has a tiny molecular radius (about 1.73 Å, and the intermolecular π-π stacking distance of OSCs is generally larger than 3.4 Å) and a large electron affinity[32] (relative to OSCs), so it can penetrate the lattice of OSCs, find an interstitial position, and play an electron-withdrawing role. Therefore, we deduce that electron transfer may occur between the neutral semiconductor molecule and oxygen, *i.e.*, oxygen works as an interstitial acceptor impurity and induces mobile hole carriers in OSCs. However, the concentration of the inherent oxygen in OSCs is at trace-levels, as confirmed by the fact that X-ray photoelectron spectroscopy (XPS) of the fresh DNTT film (without exposure in air) shows no oxygen peak signal (Supplementary Section 8). While exposed in air, a clear oxygen peak signal is observed, which suggests that the extra oxygen is adsorbed on OSCs (Supplementary Section 8). It is the easily detectable oxygen that has been extensively studied in previous work[26-30] and can be easily removed by vacuum annealing[26,27]. Quite differently, our goal is to gain an insight into the role of the trace, lattice-incorporated, oxygen that is inherent in OSCs. However, most conventional spectroscopy techniques, such as Raman, infrared, and UV-Vis absorption measurements, have limited capacity to identify the trace impurities. Therefore, to explore the role of oxygen in OSCs, we used electron paramagnetic resonance spectroscopy (EPR), a technique that has extremely low detection limits, to track unpaired electrons in the above process.

As shown in **Fig. 1d**, the fresh DNTT OFET in the static magnetic field exhibits the identifiable EPR signal with g = 2.0034 and peak-to-peak linewidth ($\triangle H_{pp}$) ≈ 5G (see Methods). The temperature dependence of the signal shows that the magnetic susceptibility (χ) obeys the Curie law (Supplementary Section 9). The signal was thus assigned to the DNTT radical cation with S = 1/2 spins in the solid state[33]. Furthermore, the spin density N_{spin} of ORC (carrier concentration) was about

1.9 × 10^{15} cm^{-3} by the Curie law (Supplementary section 9). After confirming the existence of ORC, its putative partner should be SA, but the EPR signal of SA is usually too broad to be directly observed because of fast spin relaxation. However, the presence of SA could be investigated through a spin trapping strategy using 5,5-dimethyl-1-pyrroline N-oxide (DMPO), as the SA radical trapping agent. Significantly, after the DNTT film was immersed in the DMPO diluent for 30 min (see Methods), the characteristic EPR signal of the adduct DMPO-OOH[34] of DMPO with SA was observed, with six peaks of equal height and hyperfine coupling constants A_N ≈ 13.9 G and $A_{h\beta}$ ≈ 8.8 G (**Fig. 1e**). These EPR signals are direct indicators of the existence of the geminate ORC and SA, revealing that OSCs are innately doped by trace oxygen (10^{15} cm^{-3}), and are not, as has been long assumed, intrinsic.

To further investigate the correlation between these species and OSC p-type characteristics, the EPR signals of ORC and SA (by spin trapping) in the plasma-treated OFET were examined under nitrogen protection (see Methods). As expected, no EPR signal was observed, indicating that the plasma treatment can efficiently eliminate (reduce to neutral molecules) the ionized acceptors, SA, and hole carriers, ORC. Furthermore, the EPR signals of ORC and SA were almost recovered to their initial levels after illumination in O_2 for 1 h (**Fig. 1d** and **1e**).

From the above electrical and EPR measurements, the underlying mechanism for the key role of oxygen on p-type characteristics is deduced thus: oxygen, acting as an acceptor, withdraws one electron from a neutral OSC molecule, generating SA (*i.e.*, an ionized acceptor) and ORC (*i.e.*, a hole carrier). After plasma treatment, the ORC and SA are eliminated, resulting in the disappearance of p-type characteristics, and upon illumination in oxygen, they are regenerated and thus restore the p-type characteristics. This was further supporting by first-principle molecular dynamics (FMD) and density functional theory (DFT) calculations (Supplementary Section 10). The occupancy sites of oxygen, estimated by the energy minimization principle, were estimated to be the interstitial positions in the lattice. The DFT calculations qualitatively show that the incorporation of oxygen introduces larger spatial extension of charge distribution and states distributed close to the edge of the HOMO,

causing the extended tail to shift towards a high energy level (*i.e.*, a reduction in the relative distance between E_F and the HOMO), which suggests that oxygen plays the role of an acceptor dopant in OSCs.

To elucidate these results, the energy band model of the OFET is outlined in **Fig. 2a**. Oxygen acts as an acceptor in OSCs and its states distribute along the edge of HOMO. Oxygen doping pre-empties the donor-like trap states[35] induced by static/dynamic disorder[36,37], impurity, etc. (*i.e.*, it eliminates the E_F pinning) and renders the E_F close to the edge of the HOMO (*i.e.*, it yields mobile hole carriers in the HOMO). In addition, the depletion layer at the metals/semiconductors interfaces is thin due to the oxygen doping, which facilitates carrier injection through thermionic emission (TE) and thermionic field emission (TFE)[25]. After plasma treatment, oxygen doping is eliminated, which shifts the E_F away from the HOMO and broadens the depletion layer. As a result, the concentration of hole carriers decreases sharply and TFE is suppressed, causing the decrease in conductivity (Supplementary Section 4) and off-state current (**Fig. 1b** and **c**). Furthermore, the de-doping makes the pre-emptied donor-like trap states occupied, and the carrier transport is strongly impeded by the trapping effect, causing the subthreshold swing to deteriorate. According to the multiple trapping and release (MTR) model[38], a decrease in mobility is expected. At this point, even if a large gate voltage is applied, the E_F-HOMO energy difference remains large due to the E_F pinning effect of the traps, and hence the threshold voltage dramatically increases. The above analyses qualitatively explain the decline and the ultimate disappearance of OSC p-type characteristics after plasma treatment (**Fig. 1b** and **c**, details of the discussions in Supplementary section 11).

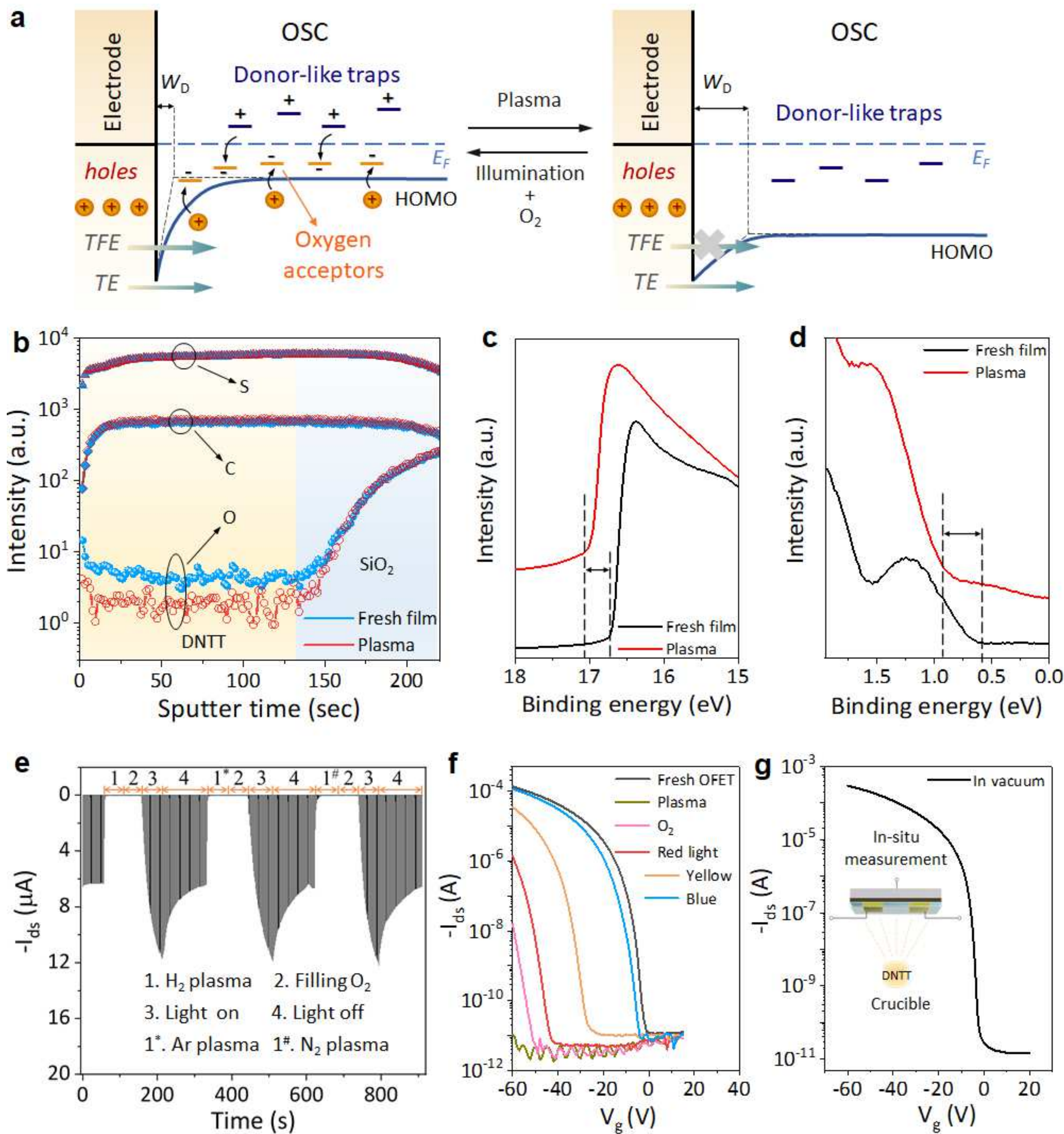

Fig. 2 | Mechanism and characteristics of the de-doping and re-doping processes. a, Band diagram of these processes. W_D is the width of the depletion layer, and TE and TFE denote thermionic emission and thermionic field emission, respectively. **b,** Intensity of the TOF-SIMS data for the C, S, and O elements of the DNTT film before and after plasma treatment, respectively. **c, d,** UPS spectra at secondary electron cut-off region (**c**) and near the Fermi-level region (**d**) of the DNTT film before and after plasma treatment, respectively. **e,** Switching cycle of the ultrathin (about 5 nm) DNTT OFET in multiple de-doping and re-doping processes with plasma treatment in H_2, Ar, and N_2. **f,** Transfer curves of the ultrathin DNTT OFET in the re-doping process under illumination at different wavelengths. **g,** Transfer curves of the bottom-contact OFET under high vacuum (in-situ measurement after evaporation of the semiconductor layer). V_{ds} = −60 V in **f and g**. Inset is the diagram of the electrical measurement of the bottom-contact OFET after the deposition of DNTT.

The removal of oxygen acceptors and the expansion of the relative gap between E_F and the HOMO can be directly proved by quasi-in-situ Time of Flight Secondary Ion Mass Spectrometry (TOF-SIMS) and Ultraviolet Photoelectron Spectra (UPS). The UPS and TOF-SIMS are connected through a vacuum pipeline (see Methods), whose environmental chamber is integrated with a plasma source. Benefiting from this, all characterizations of the DNTT film can be performed in vacuum conditions. Significantly, TOF-SIMS clearly shows the decrease of oxygen concentration after plasma treatment (**Fig. 2b**), which visually demonstrates the deoxidization effect of plasma treatment. The weak and continuous signal indicates that the trace amount of oxygen was incorporated in the lattice of OSCs rather than adsorbed on the surface. Furthermore, the secondary electron cut-off and the Fermi level both shifted about 0.35 eV towards high energy after plasma treatment (**Fig. 2c**) suggesting that the deoxidization (*i.e.*, de-doping) causes the relative gap between E_F and the HOMO to expand by about 0.35 eV, confirming the doping effect of oxygen on the OSC.

The factors influencing the de-doping and re-doping were further investigated. Firstly, the switching cycle of the ultrathin DNTT OFET was measured in the process of multiple de-doping and re-doping processes with different gas plasmas (see Methods). To accelerate the above processes, ultrathin (about 5 nm) OSC films were used, with which the de-doping and re-doping process can be repeated several times in 20 min. As shown in **Fig. 2d**, H_2, N_2, and Ar plasma show the same de-doping results, but only O_2 exposure under illumination can realize the re-doping effect. It can be deduced that the mechanism of the de-doping is that the unpaired electron of SA returns to ORC, with the energy barrier to charge transfer overcome by the plasma. This process generates the neutral semiconductor and an oxygen molecule or other oxygen-related species that escapes from the lattice through diffusion, and is very similar to the removal of H complexed with Mg in GaN by a low-energy electron beam[39]. The effect of illumination with different wavelengths on the re-doping process was also assessed (**Fig. 2e** and Supplementary Section 12). The power and exposure time of the irradiation were controlled as the wavelengths were varied, and the DNTT (bandgap absorption of about 450 nm) OFET recovery

degrees decreased in the order blue (450~435 nm) > yellow (597~577 nm) > red (760~622 nm). This implies that bandgap absorption produces excitons efficiently, and that the photoexcitation of OSCs is also a key step in the re-doping process (as shown in **Fig. 2c**). The mechanism of the re-doping can be described as follows: an OSC molecule is photoexcited, *i.e.*, an electron is excited from the HOMO to LUMO, and the electron in the excited state is energetic enough to be transferred to a nearby interstitial oxygen molecule. This process forms SA and ORC (Supplementary Section 13).

To further verify that trace oxygen is innate and stable in OSCs, a bottom-contact OFET was fabricated by vacuum evaporation (i.e., not in the presence of oxygen) and then was measured in situ. Upon the deposition of the semiconductor layer, p-type transport behavior can be observed under vacuum, as shown in **Fig. 2f**. Therefore, it can be validated that the trace oxygen is inherent in OSCs and can survive the vacuum sublimation, which is also supported by the EPR signals of the purified materials (Supplementary Section 14). Since oxygen is ubiquitous, spontaneous trace oxygen doping of OSCs may occur in the processes of material synthesis and storage. Therefore, some OSCs are 'born' with OIORC and thus endowed with p-type characteristics. Although some reports have speculated that there are unintentional dopants in OSCs[2], this is the first study to unambiguously assign and uncover the impact of these dopants.

The universality of the innate OIORC was investigated with other six typical OSCs including small molecules and polymers, with their chemical structures shown in **Fig. 3**. The EPR signals of the raw materials of these semiconductors indicate the innate existence of ORC and SA (Supplementary Section 15). All the OFETs of these semiconductors (see Methods), with different device structures (top and bottom contact) and aggregate states (single crystal and film), show the same phenomena as the DNTT OFET (**Fig. 1b** and **c**) in the processes of plasma treatment and illumination in oxygen (**Fig. 3a-f**). These results reveal the same origin of p-type characteristics in OSCs (*i.e.*, OIORC) and demonstrate the university of the de-doping and re-doping methods. The incomplete elimination of p-type characteristics for single crystal rubrene and the C_8-BTBT crystalline film after plasma treatment

may be due to the serious suppression of the short-circuit diffusion for the plasma and oxygen in thick crystals.

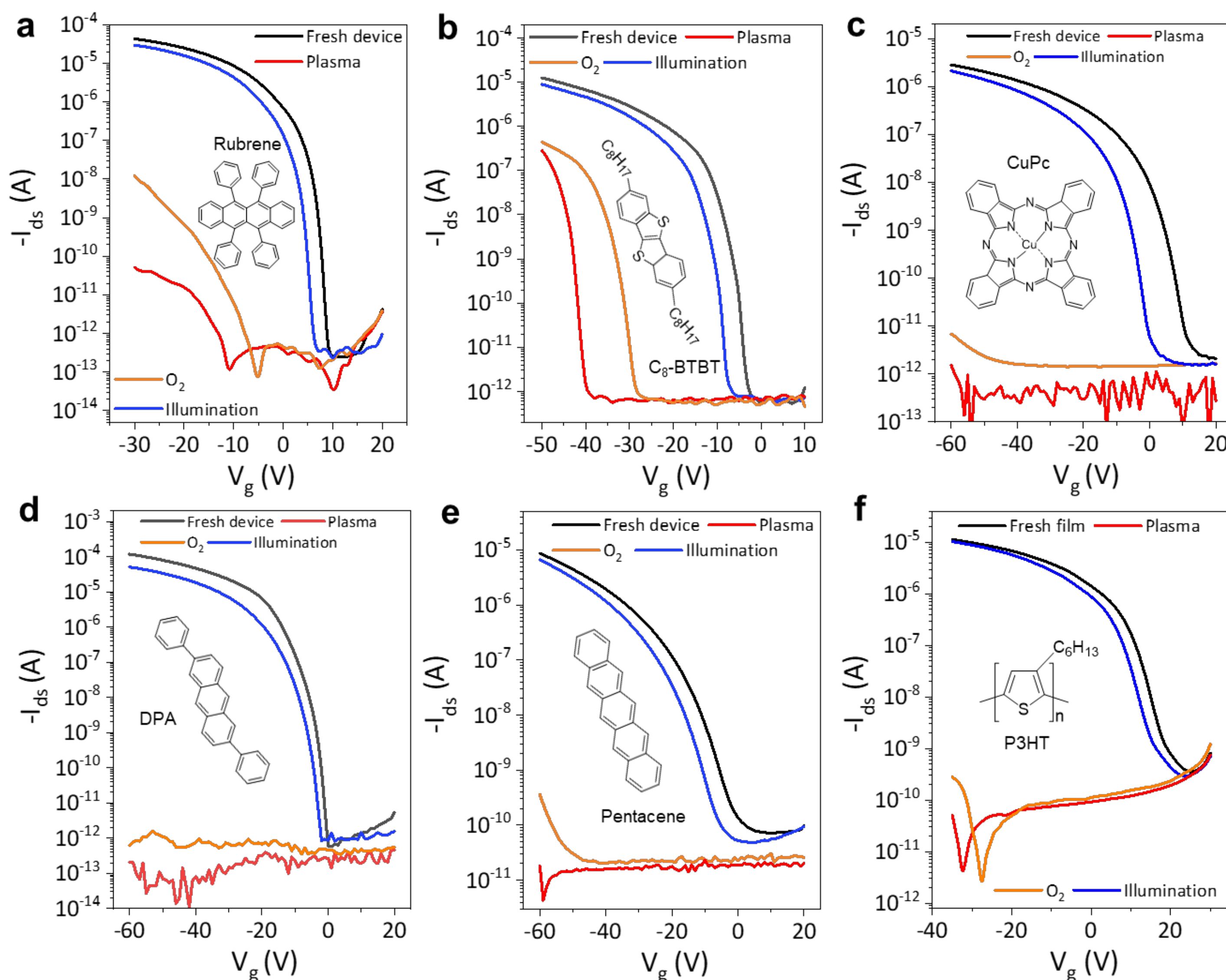

Fig. 3 | Molecular universality of the de-doping and re-doping phenomenon (*i.e.*, universality of the innate trace oxygen doping in OSCs). a-f, Transfer curves in the saturation region of the OFET of rubrene, C8-BTBT, CuPc, DPA, pentacene and P3HT in the de-doping and re-doping process. The insets are the corresponding molecular structures.

It is well-known that controlled doping is the core technique enabling the fine control of semiconducting characteristics in inorganic electronics. To demonstrate the potential applications of the reversible de-doping and re-doping methods in organic electronic devices, three kinds of tests for modulating key device parameters were performed:

1) The threshold voltage (V_{th}) is a vital parameter for transistors, and precise V_{th} control can be achieved for inorganic semiconductors through ion implantation (a doping technique)[25], but this has

been a challenge in organic electronics[40]. As shown in **Fig. 4a** and **b**, 14 OFETs with a negative V_{th} and 14 OFETs with a positive V_{th} were all carefully modulated to turn on at about 0 V, without any observed decrease in mobility, by tuning the doping density by plasma treatment, and simultaneous annealing and illumination in oxygen (see Methods), respectively. These results show that the de-doping and re-doping methods have great potential for the precise control of the threshold voltage in organic electronics

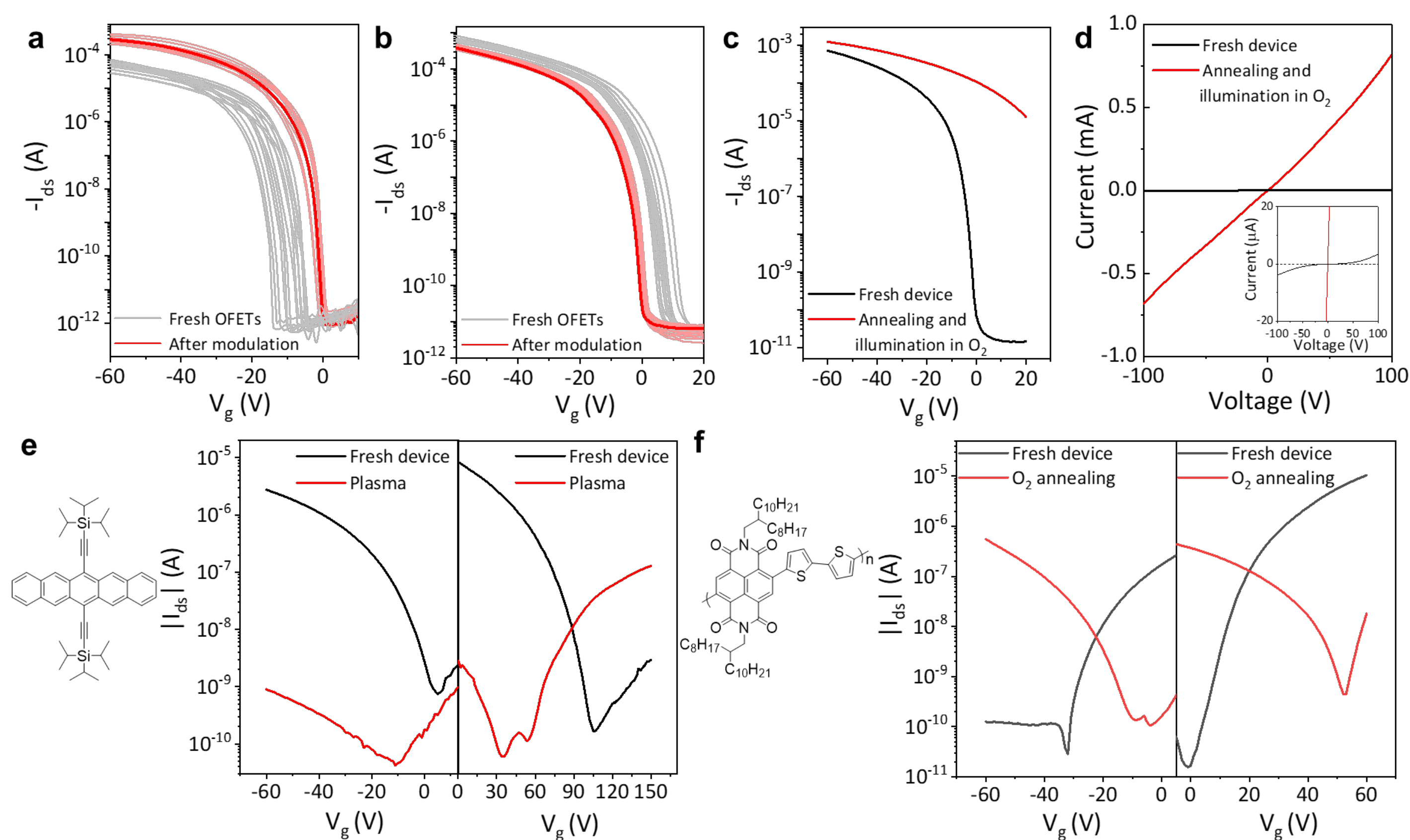

Fig. 4 | Applications of the de-doping and re-doping methods. a, b, Precise modulation of the threshold voltage of the DNTT OFETs (from negative (**a**) and positive (**b**) values to near zero). **c, d**, Increase of the conductivity of the DNTT film by oxygen doping. Transfer curves (**c**) and I-V curves (**d**) before and after annealing and illuminating in O_2. The inset is the enlarged view of the current of **d**. **e, f**, Modification of the polarity of p-type (**e**, tips-pentacene) and n-type (**f**, P(NDI2OD-T2)) OSCs. The transfer characteristics were measured in the saturation region.

2) Control of doping concentration is crucial for tuning the junction properties and conductivity in electronic devices. Remarkably, efficient doping with almost no decrease of mobility of small molecule films can be achieved by oxygen doping. After simultaneous annealing (80 ºC) and illumination in 3 atm of oxygen for 3 h, the C_{10}-DNTT OFET changed from accumulation mode to depletion mode and

showed weak dependence on gate voltage (**Fig. 4c**). Notably, the conductivity (σ) sharply increased over two orders of magnitude to 72 S m^{-1}, and the field-effect mobility (μ) showed only a slight decrease (5.2 to 3.6 $cm^2 \cdot V^{-1} \cdot s^{-1}$). With these data, the carrier density n was calculated as 2×10^{18} cm^{-3} (using $\sigma = ne\mu$), which is a high doping level for small molecule OSCs (molecular density about 10^{21} cm^{-3}). In addition, the I-V curve was transformed from nonlinearity to linearity (**Fig. 4d**), indicating the obvious improvement of metal-semiconductor junctions under high concentration doping.

3) The polar type of the transport behaviors can be modified by oxygen doping and de-doping. OSCs are intrinsically ambipolar, but the innate oxygen doping generally compensates for the electrons. However, we hypothesized that p-type materials could appear n-type after eliminating oxygen and, conversely, n-type materials could be converted to be p-type through further oxygen doping. For the former case, we showed that an OFET of tips-pentacene, showing p-type transport behavior both in air and vacuum, was modified to be n-type *via* de-doping by plasma treatment (**Fig. 4e**). For the latter case, we showed that P(NDI2OD-T2), a stable and high-performance n-type polymer[41], was endowed with p-type behavior *via* doping by simultaneous annealing and illumination in oxygen (**Fig. 4f**). Although similar re-doping methods have been reported, due to the lack of a de-doping method for the removal of lattice-incorporated oxygen, full control of the vital parameters of OSCs and devices could not be realized by the re-doping method alone. These experiments demonstrate the power and utility of the de-doping and re-doping processes; dramatically widening the possible OSC charge transport property space without introducing any new materials.

With the lack of an effective trace oxygen de-doping strategy, as outlined in this study, it is understandable that the p-type charge transport in OSCs was considered intrinsic in origin, and why oxygen doping was always considered an additional influence on the 'inherent' p-type characteristics[26-30]. Based on this incorrect premise, many phenomena, and properties of OSCs and photo-electronic devices have been studied and reported, which, in fact, might be strongly affected by the innate oxygen doping. In this light, some classical physical models for the quantitative description

of organic devices are invalid, such as depletion approximation theory[25,42] and Debye length calculations[34], both of which require the estimation of doping concentration. We believe this work will help to correctly use these models, clarify previously perplexing key organic electronics phenomena, and push forward OSCs material research:

1) Depletion-mode transistors[4,5], carrier densities[6,10] and conductivities beyond expectation[2,9,43], and the small energy gap between the E_F and the HOMO[7,8] can be easily interpreted by oxygen-induced excess hole carriers. This also explains the difficulty of inversion of polarity for OSCs[44].

2) The deterioration of subthreshold swing (S) at low temperature[11,12] was previously unclear. Ideally, S should improve at low temperature due to the relationship: $S \equiv (ln10)\frac{dV_g}{d(lnI_{ds})} = (ln10)\left(\frac{C_i+C_t}{C_i}\right)\frac{kT}{q}$, where C_i and C_t are capacitance of dielectric layer and traps, respectively[45]. However, experimentally, the S value always increases at low temperature in OFETs. This can be explained by the freeze-out effect; at low temperature, the carriers (ORCs) are frozen around the impurities (oxygen) (*i.e.*, impurities are not ionized), and thus the trap states passivated by oxygen doping recover the ability of trapping field-induced (gate voltage) carriers, which increases the trap capacitance and thus deteriorates S.

3) These findings may inspire the research on the origin of n-type characteristics in OSCs. We anticipate that an unrevealed impurity is prevalent in n-type OSCs, just like oxygen, and passivates the acceptor-like traps and induces mobile electron carriers in the LUMO.

Our study reveals, through a low-power plasma de-doping strategy, that trace oxygen is the origin of the p-type characteristics of OSCs. This finding explains previously perplexing organic electronics phenomena and will enable a foundation upon which we can re-understand charge transport in OSCs. Furthermore, our de-doping and re-doping processes will expand the property space for all known OSC materials and, we believe, will become a core technology for the growing organic electronics industry.

References

1 Zaumseil, J. & Sirringhaus, H. Electron and Ambipolar Transport in Organic Field-Effect Transistors. *Chem. Rev.* **107**, 1296-1323, (2007).

2 Jacobs, I. E. & Moulé, A. J. Controlling Molecular Doping in Organic Semiconductors. *Adv. Mater.* **29**, 1703063, (2017).

3 Zhao, W. *et al.* Chemical doping of organic semiconductors for thermoelectric applications. *Chem. Soc. Rev.* **49**, 7210-7228, (2020).

4 Horowitz, G., Hajlaoui, R. & Kouki, F. An analytical model for the organic field-effect transistor in the depletion mode. Application to sexithiophene films and single crystals. *Eur. Phys. J. AP* **1**, 361-367, (1998).

5 Scharnberg, M. *et al.* Tuning the threshold voltage of organic field-effect transistors by an electret encapsulating layer. *Appl. Phys. Lett.* **90**, 013501, (2007).

6 Kaji, T., Takenobu, T., Morpurgo, A. F. & Iwasa, Y. Organic Single-Crystal Schottky Gate Transistors. *Adv. Mater.* **21**, 3689-3693, (2009).

7 Ellison, D. J., Lee, B., Podzorov, V. & Frisbie, C. D. Surface Potential Mapping of SAM-Functionalized Organic Semiconductors by Kelvin Probe Force Microscopy. *Adv. Mater.* **23**, 502-507, (2011).

8 Greiner, M. T. *et al.* Universal energy-level alignment of molecules on metal oxides. *Nat. Mater.* **11**, 76-81, (2012).

9 Salzmann, I. *et al.* Molecular Electrical Doping of Organic Semiconductors: Fundamental Mechanisms and Emerging Dopant Design Rules. *Acc. Chem. Res.* **49**, 370-378, (2016).

10 Huang, Y. *et al.* Effectively modulating thermal activated charge transport in organic semiconductors by precise potential barrier engineering. *Nat. Commun.* **12**, 21, (2021).

11 Minari, T., Nemoto, T. & Isoda, S. Temperature and electric-field dependence of the mobility of a single-grain pentacene field-effect transistor. *J. Appl. Phys.* **99**, 034506, (2006).

12 Mei, Y. *et al.* Crossover from band-like to thermally activated charge transport in organic transistors due to strain-induced traps. *Proc. Natl. Acad. Sci. U.S.A.* **114**, E6739-E6748, (2017).

13 Xu, J. *et al.* Highly stretchable polymer semiconductor films through the nanoconfinement effect. *Science* **355**, 59-64, (2017).

14 Hou, L. *et al.* Optically switchable organic light-emitting transistors. *Nature Nanotechnology* **14**, 347-353, (2019).

15 Yamashita, Y. *et al.* Efficient molecular doping of polymeric semiconductors driven by anion exchange. *Nature* **572**, 634-638, (2019).

16 Kong, J. *et al.* CO_2 doping of organic interlayers for perovskite solar cells. *Nature* **594**, 51-56, (2021).

17 Sakai, N. *et al.* Adduct-based p-doping of organic semiconductors. *Nat. Mater.* **20**, 1248-1254, (2021).

18 Yang, F. *et al.* Vertical-organic-nanocrystal-arrays for crossbar memristors with tuning switching dynamics toward neuromorphic computing. *SmartMat* **2**, 99-108, (2021).

19 Ai, X. *et al.* Efficient radical-based light-emitting diodes with doublet emission. *Nature* **563**, 536-540, (2018).

20 Kanagasekaran, T. *et al.* A new electrode design for ambipolar injection in organic semiconductors. *Nat. Commun.* **8**, 999, (2017).

21 Tang, C. G. *et al.* Multivalent anions as universal latent electron donors. *Nature* **573**, 519-525, (2019).

22 Chua, L.-L. *et al.* General observation of n-type field-effect behaviour in organic semiconductors. *Nature* **434**, 194-199, (2005).

23 Nicolai, H. T. *et al.* Unification of trap-limited electron transport in semiconducting polymers. *Nat. Mater.* **11**, 882-887, (2012).

24 Ren, Y. *et al.* Recent Advances in Ambipolar Transistors for Functional Applications. *Adv. Funct. Mater.* **29**, 1902105, (2019).

25 Sze, S. M. & Ng, K. K. *Physics of Semiconductor Devices*. (John wiley & sons, 2006).

26 Abdou, M. S. A., Orfino, F. P., Son, Y. & Holdcroft, S. Interaction of Oxygen with Conjugated Polymers: Charge Transfer Complex Formation with Poly(3-alkylthiophenes). *J. Am. Chem. Soc.* **119**, 4518-4524, (1997).

27 Maliakal, A. J. *et al.* Mechanism for Oxygen-Enhanced Photoconductivity in Rubrene: Electron Transfer Doping. *Chem. Mater.* **21**, 5519-5526, (2009).

28 Mitrofanov, O. *et al.* Oxygen-Related Band Gap State in Single Crystal Rubrene. *Phys. Rev. Lett.* **97**, 166601, (2006).

29 Najafov, H. *et al.* Photon-Assisted Oxygen Diffusion and Oxygen-Related Traps in Organic Semiconductors. *Adv.*

Mater. **23**, 981-985, (2011).
30 Lu, G. *et al.* Moderate doping leads to high performance of semiconductor/insulator polymer blend transistors. *Nat. Commun.* **4**, 1588, (2013).
31 Yamamoto, T. & Takimiya, K. Facile Synthesis of Highly π-Extended Heteroarenes, Dinaphtho[2,3-b:2‘,3‘-f]chalcogenopheno[3,2-b]chalcogenophenes, and Their Application to Field-Effect Transistors. *J. Am. Chem. Soc.* **129**, 2224-2225, (2007).
32 Tang, C. G. *et al.* Doped polymer semiconductors with ultrahigh and ultralow work functions for ohmic contacts. *Nature* **539**, 536-540, (2016).
33 Matsui, H. *et al.* Correlation between interdomain carrier hopping and apparent mobility in polycrystalline organic transistors as investigated by electron spin resonance. *Phys. Rev. B* **85**, 035308, (2012).
34 Clément, J.-L. *et al.* Assignment of the EPR Spectrum of 5,5-Dimethyl-1-pyrroline N-Oxide (DMPO) Superoxide Spin Adduct. *J. Org. Chem.* **70**, 1198-1203, (2005).
35 Haneef, H. F., Zeidell, A. M. & Jurchescu, O. D. Charge carrier traps in organic semiconductors: a review on the underlying physics and impact on electronic devices. *J. Mater. Chem. C* **8**, 759-787, (2020).
36 Lee, B. *et al.* Trap healing and ultralow-noise Hall effect at the surface of organic semiconductors. *Nat. Mater.* **12**, 1125-1129, (2013).
37 Burlingame, Q. *et al.* Centimetre-scale electron diffusion in photoactive organic heterostructures. *Nature* **554**, 77-80, (2018).
38 Podzorov, V. *et al.* Intrinsic Charge Transport on the Surface of Organic Semiconductors. *Phys. Rev. Lett.* **93**, 086602, (2004).
39 Nakamura, S. The Roles of Structural Imperfections in InGaN-Based Blue Light-Emitting Diodes and Laser Diodes. *Science* **281**, 956-961, (1998).
40 Kergoat, L. *et al.* Tuning the threshold voltage in electrolyte-gated organic field-effect transistors. *Proc. Natl. Acad. Sci. U.S.A.* **109**, 8394-8399, (2012).
41 Yan, H. *et al.* A high-mobility electron-transporting polymer for printed transistors. *Nature* **457**, 679-686, (2009).
42 Takshi, A., Dimopoulos, A. & Madden, J. D. Depletion width measurement in an organic Schottky contact using a metal-semiconductor field-effect transistor. *Appl. Phys. Lett.* **91**, 083513, (2007).
43 Lüssem, B. *et al.* Doped Organic Transistors. *Chem. Rev.* **116**, 13714-13751, (2016).
44 Lee, T. H. *et al.* p-Channel Field-Effect Transistors Based on C60 Doped with Molybdenum Trioxide. *ACS Appl. Mater. Inter.* **5**, 2337-2341, (2013).
45 Blülle, B., Häusermann, R. & Batlogg, B. Approaching the Trap-Free Limit in Organic Single-Crystal Field-Effect Transistors. *Phys. Rev. Appl.* **1**, 034006, (2014).

Methods

Fabrication of OFETs

OSCs were purchased from Sigma-Aldrich, Shanghai Daeyeon Chemicals, and TCI Chemicals and were purified by physical vapor transport three times (except P3HT). The semiconductors in different batches and from different companies exhibited the same phenomena. OFETs in this work adopted a bottom-gate top-contact configuration, unless otherwise stated in the text. The highly doped Si wafers (500 μm thick) with a 300-nm-thick thermal oxide layer were treated by oxygen plasma (100 W, 30 s) to produce hydroxyl groups, and then modified with octadecyltrichlorosilane (OTS, purchased from

Aldrich) in vacuum oven for 1 h at 120 ºC. The films of DNTT, C_{10}-DNTT, PEN, CuPc were vapor deposited on the OTS-treated SiO_2/Si surface at a rate of 0.1 Å s^{-1} below 10^{-4} Pa (achieving a usual thickness of 20-30 nm), and substrate temperature was kept between 60-100 ºC. A 20 nm layer of Au was deposited as the source-drain electrodes through a shadow mask under a vapor deposition rate of about 0.005 nm s^{-1}. The ultrathin DNTT film (about 5 nm) was vapor deposited on the polystyrene (PS)-coated SiO_2/Si (5 mg ml^{-1} in toluene, spin-coated on SiO_2 at 3000 rpm for 1 min by a KW-4A, Setcas) at a rate of 0.02 Å s^{-1}, and the substrate was kept at room temperature. Note that the uniformity and stability of the ultrathin films were usually poor, so regular thickness films were used for most of this work. All deposition processes were performed in the vacuum thermal evaporation system connected to an N_2 glovebox, convenient for the storage of devices in an oxygen-free environment. To fabricate the bottom-gate bottom-contact OFET, 20 nm Au electrodes were deposited on OTS-treated SiO_2/Si, and then modified with pentafluorobenzenethiol (PFBT, purchased from Aldrich) by immersing into a 10 mM solution of PFBT in 2-propanol for 5 min. Leading wires were then bonded on the source-drain electrodes and gate for in-situ measurement before DNTT deposition. In addition, a rubrene single crystal was grown by physical vapor transport, and then transferred onto a prefabricated polymethyl methacrylate (PMMA)/Si stamp with an air gap. PMMA (10 mg ml^{-1} in toluene) was spin-coated on the highly doped Si at 800 rpm for 1 min, and then 20 nm Au was deposited on PMMA/Si. The air gap was fabricated by mechanical scraping using a probe. The C_8-BTBT crystalline film was prepared by the space-confined self-assembly method[46], and the Au (80 nm) stripes were stamped on the C_8-BTBT crystalline film as the source and drain electrodes[47].

In-situ Electrical characterizations

The electrical characterizations of the OFETs were carried out in a home-made system integrated with a DC inductively coupled plasma source, an optical window and the environmental control system (Supplementary Section 2) using two types of semiconductor device analyzers (an Agilent B1500A and a PDA FS380). The home-made system is connected to an N_2 glovebox. The leading wires were

bonded on the source-drain electrodes and the gate electrode by a wire bonder. The environmental control system controlled the type and velocity of the filling gases and modulated the atmospheric pressure in the range of 10^{-5}-10^{5} Pa. Purified gases (99.999%) for plasma treatment were further purified by the dehydration tube and deoxygenation tube in series. The plasma source normally worked on low power (below 20 W). The time of the plasma treatment for de-doping was usually below 1 min. Illumination was performed using a Xe lamp (adjustable power of 0-300 W) and an LED Light (15 W) with switchable wavelength (450~435 nm, 597~577, 760~622 nm). In the de-doping and re-doping investigations, the OFETs were measured about 1 min after the plasma treatment and examined about 3 min after illumination in O_2 (to avoid the influence of photogenerated carriers on the results). The switching cycle of the ultrathin (about 5 nm) DNTT OFET in the multiple de-doping and re-doping process was measured by a PDA FS380. V_{ds} was set to -30 V and V_{gs} was switched from 0 to -30 V with intervals of 1 s. The power of the plasma was set to 1 W. The measurement of the bottom-contact OFET was performed in the vacuum thermal evaporation system with electrical interfaces. Then, the OFET was transferred to the probe stand in an N_2 glovebox. During the 3 days storage (with several hours of illumination), the transfer curve was measured multiple times and showed negligible change.

EPR characterizations

X-band (9.5 GHz) electron paramagnetic resonance (EPR) measurements were performed with both a Bruker EMXplus-6/1 and JEOL JES-FA200. The microwave power and the modulation magnetic field were carefully adjusted to produce the optimal EPR signal. DNTT films were deposited onto a 3.5 mm wide × 20 mm long quartz substrate. The sample was then inserted into a quartz EPR tube. The signal of the DNTT film is usually weak due to the larger spin-orbit coupling caused by the sulfur atoms[48]. The signal intensity can be improved by increasing the quantity of samples. For low-temperature measurements, a continuous liquid nitrogen flow cryostat was used. 2,2-Diphenyl-1-picrylhydrazyl (DPPH) was used as a standard spin counting reference. For the detection of the

superoxide anion (SA), DMPO (volume ratio of 1:100 in methanol or dimethylsulphoxide) was used as a spin trapping agent. To boost the signal intensity, multiple DNTT films were immersed into DMPO diluent for at least 30 min. The solution was sucked up with a glass capillary and inserted into a quartz EPR tube. To track unpaired electrons in the de-doping process, the plasma-treated DNTT film (not exposed to the air) was inserted into a quartz EPR tube in the N_2 glovebox and then the tube was sealed with silicone grease. The samples for SA detection of the plasma-treated DNTT films were prepared and sealed in the glovebox as described above. Note that purified gases (99.999%) for plasma treatment needed to be further purified by the dehydration tube and deoxygenation tube in series. To investigate the re-doping process, the plasma-treated DNTT films were illuminated in O_2 with a Xe lamp for 24 h, and then the tests were performed as above. For the detection of raw materials, OSCs powders or suspensions blended into DMPO diluent were loaded into glass capillaries. After being sealed with silicone grease, the glass capillaries were inserted into a quartz EPR tube. Some weak signals were carefully denoised.

Quasi-in-situ UPS and TOF-SIMS characterizations

UPS (PHI 5000 Versaprobe II) and TOF-SIMS (TOF.SIMS5-100) are connected through a vacuum pipeline, whose environmental chamber (which controls the gas type and the atmospheric pressure) is integrated with a plasma source. DNTT films (about 50 nm) were deposited onto the highly doped Si and SiO_2/Si for UPS and TOF-SIMS tests, respectively. The excitation source for UPS was He Iα (hv = 21.22 eV). Vacuum level shifts were determined from the low kinetic energy part of UPS spectra with a -5 V sample bias. Secondary ions employed Cs^+ as the primary ion source. The size of the crater was 100 × 100 um, and the area of acceptance was 25% of the total sputtered area. The UPS and TOF-SIMS tests were performed on the fresh DNTT films in turn, and they were returned to the environmental chamber through a vacuum pipeline to be treated by plasma with purified gas (gas was further purified by the dehydration tube and deoxygenation tube in series). The plasma-treated DNTT films were transferred to the UPS and TOF-SIMS in turn through a vacuum pipeline for testing. All the

transfer processes of samples were carried out in vacuum. The in-situ test equipment and technology supports were provided by NANO-X (Vacuum Interconnected Nanotech Workstation) in Suzhou.

Morphology, physical phase, and chemical structure characterizations

Morphology, physical phase, and chemical structure characterizations on the DNTT films were performed before and after plasma treatment. AFM measurements were carried out on a Dimension ICON (Bruker). XRD measurements were carried out on a MiniFlex600 (Rigaku). DNTT films were deposited on a quartz plate for the measurement of the UV-Vis absorption spectrum (a Lambda 750) and deposited on Au-coated Si for the measurements of the Raman spectrum (a DXR Microscope with a 532 nm laser), and IR spectrum (Nicolet IN10, Thermo Fisher Scientific). A 50 nm DNTT film was deposited on highly doped Si in a vacuum thermal evaporation system and transferred under the protection of N_2 to an Ar glovebox connected to an ESCALAB-250Xi (Thermo Fisher Scientific).

Modulation of the key device parameters

Threshold voltage: In-situ electrical measurements were performed on 14 DNTT (20-30 nm) OFETs with negative V_{th} after plasma treatment. The parameters of the plasma treatment were carefully modulated until the V_{th} was tuned at about 0 V. Correspondingly, 14 DNTT OFETs with positive V_{th} were repeatedly measured after simultaneous annealing and illumination in oxygen until the V_{th} was tuned at about 0 V.

Conductivity: The C_{10}-DNTT OFET was annealed at 80 ºC in a cavity with an inspection window, and O_2 was filled into the cavity with a pressure of about 3 atm. Illumination was performed by a Xe lamp.

Polarity: The Tips-pentacene film was prepared by the drop-casting method (1 mg ml^{-1} in toluene) onto the PS-coated SiO_2/Si and then Au was deposited as electrodes. The P(NDI2OD-T2) film was prepared by spin-coating onto OTS-treated SiO_2/Si and Au was also used as electrodes. The Tips-pentacene OFET was treated by plasma at 20 W for 1 min and P(NDI2OD-T2) OFET was annealed at 60 ºC and illuminated in O_2 for 3 h.

Data availability

The data presented in this study are available from the corresponding authors.

Methods References

46 Wang, Q. *et al.* Space-Confined Strategy toward Large-Area Two-Dimensional Single Crystals of Molecular Materials. *J. Am. Chem. Soc.* **140**, 5339-5342, (2018).

47 Tang, Q. *et al.* High-Performance Air-Stable Bipolar Field-Effect Transistors of Organic Single-Crystalline Ribbons with an Air-Gap Dielectric. *Adv. Mater.* **20**, 1511-1515, (2008).

48 Schott, S. *et al.* Tuning the effective spin-orbit coupling in molecular semiconductors. *Nat. Commun.* **8**, 15200, (2017).

Acknowledgements

The authors are grateful to National Key Research and Development Program (2018YFA0703200, 2016YFB0401100), National Natural Science Foundation of China (52073210, 21905199, 21573277, 51633006), Natural Science Foundation of Tianjin City (19JCZDJC37400, 194214030036), and Key Research Program of Frontier Sciences of Chinese Academy of Sciences (QYZDB−SSW−SLH031). The authors sincerely appreciate the technological support from Vacuum Interconnected Nanotech Workstation (NANO-X), Suzhou Institute of Nano-Tech and Nano-Bionics (SINANO), Chinese Academy of Sciences, and Prof. Yi Cui, Dr. Xuefei Weng, Dr. Rong Huang, Gongzhong Miao, Zhiyun Li in NANO-X.

Author contributions

L.L. and Y.H. discovered the oxygen de-doping and re-doping of organic semiconductors and conceived the experiments. K.W. found the acceleration effect of illumination on re-doping. Y.H. and X.C. performed the device fabrication, electrical and spectral characterizations, and developed the controlled doping and de-doping technologies. Y.S. conducted the theoretical calculations. Z.W., Y.H., L.Y., S.W., J.L., D.J., X.Z., and H.D. assisted in the experiments. L.L., Y.H., X.C., and W.H. conceived, analyzed, and wrote the manuscript. W.H. supervised the work.

Competing interests

The authors declare no competing interests.

Additional information

Supplementary Information accompanies this paper at XXX.

Correspondence and requests for materials should be addressed to Wenping Hu.

Reprints and permissions information is available at http://www.nature.com/reprints.

Supplementary Files

This is a list of supplementary files associated with this preprint. Click to download.

- Supplementaryinformation1027.docx